NeuroImage 125 (2016) 533–543

Contents lists available at ScienceDirect

NeuroImage

journal homepage: www.elsevier.com/locate/ynimg

Direct detection of optogenetically evoked oscillatory neuronal electrical activity in rats using SLOE sequence

Yuhui Chai [a,b], Guoqiang Bi [c], Liping Wang [d], Fuqiang Xu [e,f], Ruiqi Wu [e,f], Xin Zhou [e], Bensheng Qiu [g], Hao Lei [e], Yaoyu Zhang [a,b], Jia-Hong Gao [a,b,h,*]

[a] Beijing City Key Lab for Medical Physics and Engineering, Institute of Heavy Ion Physics, School of Physics, Peking University, Beijing, People's Republic of China
[b] Center for MRI Research, Academy for Advanced Interdisciplinary Studies, Peking University, Beijing, People's Republic of China
[c] School of Life Sciences, University of Science and Technology of China, Hefei, People's Republic of China
[d] Shenzhen Institutes of Advanced Technology, Chinese Academy of Sciences, Shenzhen, People's Republic of China
[e] Wuhan Institute of Physics and Mathematics, Chinese Academy of Sciences, Wuhan, People's Republic of China
[f] CAS Center for Excellence in Brain Science and Intelligence Technology, Chinese Academy of Sciences, People's Republic of China
[g] School of Information Science and Technology, University of Science and Technology of China, Hefei, People's Republic of China
[h] McGovern Institute for Brain Research, Peking University, Beijing, People's Republic of China

ARTICLE INFO

Article history:
Received 4 August 2015
Accepted 20 October 2015
Available online 27 October 2015

Keywords:
Neuronal current
Neuronal electrical activity
Oscillatory current
Spin-lock
Functional MRI
Optogenetics

ABSTRACT

The direct detection of neuronal electrical activity is one of the most challenging goals in non-BOLD fMRI research. Previous work has demonstrated its feasibility in phantom and cell culture studies, but attempts in in vivo studies remain few and far between. Most recent in vivo studies used T2*-weighted sequences to directly detect neuronal electrical activity evoked by sensory stimulus. As neuronal electrical signal is usually comprised of a series of spectrally distributed oscillatory waveforms rather than being a direct current, it is most likely to be detected using oscillatory current sensitive sequences. In this study, we explored the potential of using the spin-lock oscillatory excitation (SLOE) sequence with spiral readout to directly detect optogenetically evoked oscillatory neuronal electrical activity, whose main spectral component can be manipulated artificially to match the resonance frequency of spin-lock RF field. In addition, experiments using the stimulus-induced rotary saturation (SIRS) sequence with spiral readout were also performed. Electrophysiological recording and MRI data acquisition were conducted on separate animals. Robust optogenetically evoked oscillatory LFP signals were observed and significant BOLD signals were acquired with the GE-EPI sequence before and after the whole SLOE and SIRS acquisitions, but no significant neuronal current MRI (ncMRI) signal changes were detected. These results indicate that the sensitivity of oscillatory current sensitive sequences needs to be further improved for direct detection of neuronal electrical activity.

1. Introduction

Blood-oxygenation-level-dependent (BOLD) contrast was first described by Ogawa in 1990 (Ogawa et al., 1990), and rapidly became widely used for noninvasive detection and mapping of human brain activities. Unfortunately due to its indirect detection of neuronal activation through neurovascular coupling, the temporal resolution and spatial accuracy for mapping of neuronal activities with this technique are limited. In contrast, electroencephalography (EEG) and magnetoencephalography (MEG) directly measure the scalp electric and magnetic fields, respectively, originating from brain activities, and offer excellent temporal resolution at the millisecond level. However, a major barrier to the determination of neuronal substrates of the EEG/MEG signal is the inverse problem: EEG/MEG map with a certain distribution recorded at the scalp cannot lead to a unique solution for the source location (Lopes da Silva, 2004). It has been proposed that simultaneous EEG-fMRI could overcome the spatial limitations of EEG and temporal limitations of fMRI (Ritter and Villringer, 2006). However, the neuronal dynamics detected at the surface of a skull by EEG/MEG only reflects the general sum of the whole brain rather than a particular neuronal electrical activity at the voxel level.

To overcome these limitations, a hope among brain imagers is to use MRI to directly detect the neuronal magnetic field (NMF) generated by neuronal electrical activity with high spatiotemporal resolution. Such an approach has been termed as neuronal current MRI (ncMRI) and intense efforts have been made to determine the extent to which such an undertaking is feasible. Resembling BOLD contrast, most recent studies of ncMRI were based on the detection of a phase shift or dephasing of the MRI signal created by extremely weak NMF. As neuronal electrical signal is usually comprised of a series of spectrally distributed oscillatory

* Corresponding author at: Center for MRI Research, Peking University, Beijing 100871, Peoples Republic of China.
E-mail address: jgao@pku.edu.cn (J.-H. Gao).

http://dx.doi.org/10.1016/j.neuroimage.2015.10.058
1053-8119/

waveforms rather than being a direct current (Buzsaki et al., 2012), this method requires that the discharging duration of neuronal activity must be carefully aligned with the MRI acquisition window to minimize cancelation of the induced phase of biphasic or multi-phasic NMF. For GE-EPI, the most typically used sequence in recent ncMRI acquisitions, TE period should be limited to a portion of a single phase of NMF. And for SE-EPI, timing of the 180° pulse must be set to the changing point of the biphasic signal (Singh, 1994). So far, although the feasibility of ncMRI has been demonstrated in phantom (Konn et al., 2003) and in vitro studies (Petridou et al., 2006), attempts in in vivo studies remain few and far between (Bianciardi et al., 2004; Konn et al., 2003; Liston et al., 2004; Luo et al., 2009; Park et al., 2004; Sundaram et al., 2010; Xiong et al., 2003; Xue et al., 2009).

Recently, the emergence of a technique that is sensitive to oscillatory or multiphasic neuronal electrical activity has advanced the ncMRI technology. Oscillatory neuronal electrical activity with a major spectral component matching the resonance frequency of the spin-lock field (f_{SL}) is capable of inducing rotary saturation of the spin-locked magnetization. This process is known as stimulus-induced rotary saturation (SIRS), and the feasibility of using it to measure oscillatory electrical activity has been demonstrated in phantom studies (Witzel et al., 2008). Compared with GE-EPI, SIRS is insensitive to phase cancelation in the time domain while maintaining the same level of sensitivity (Witzel et al., 2008). Building on the SIRS approach, Jiang et al. (2015) proposed to apply oscillatory electrical activity as the excitation pulse during the spin-lock time (T_{SL}), termed as spin-lock oscillatory excitation (SLOE). Phantom studies were performed to demonstrate that a 100 Hz sinusoidal magnetic field with a magnitude as low as 0.25 nT could be robustly detected using a 3 T MRI scanner. The dramatically improved sensitivity of field strength at the sub-nanotesla level is close to the in vivo NMF condition, and hence makes in vivo ncMRI a realistic prospect. Despite all the great advantages of the SLOE and SIRS methods mentioned above, no in vivo study using either method has been published yet.

To explore the feasibility of using SLOE and SIRS methods to detect NMF in vivo, an oscillatory neuronal electrical activity meeting the following requirements is needed. First more power concentrated in a narrow frequency band is better for the spin-lock effect. The full width at half maximum (FWHM) of saturation spectra for both SLOE and SIRS methods is only about 6 Hz (Jiang et al., 2015; Witzel et al., 2008), and the spectral components of the oscillatory electrical activity outside of the spin-lock FWHM contribute little to rotary saturation. Second the timing of the oscillatory neuronal electrical activity should ideally be controllable and predictable. Only oscillatory electrical activity during the spin-lock period contributes to rotary saturation, and the magnitude and sign of the contrast are dependent on the initial phase of the oscillatory waveform using SLOE method. Therefore the timing of the spin-lock module should be properly predefined to capture the oscillatory neuronal electrical activity. Optogenetically evoked oscillatory neuronal electrical activity meets the above two requirements. With the light-sensitive protein channelrhodopsin (ChR2) expressed in neuronal membrane, light at a specific wavelength can induce neuronal electrical activity directly. Consequently, the main spectral component of the optogenetically evoked oscillatory electrical activity can be manipulated to be on resonance with the spin-lock RF field, and the timing of the electrical activity can be adjusted to be aligned with the spin-lock period at millisecond accuracy. The word “oscillatory” in this study is used to describe the waveform shape of the electrical signal and is different from neuronal oscillation, which is a specific definition in neuroscience.

In this study, we used SLOE sequence with spiral readout to directly detect optogenetically evoked oscillatory neuronal electrical activity in rats. In addition, experiments using SIRS sequence with spiral readout were also performed. As the contrasts of SLOE and SIRS methods come from the spin-lock preparation, spin relaxation during echo time (TE) only decays the contrast. So less TE gives better contrast, and spiral readout will provide a smaller minimum TE than EPI readout. By utilizing optical stimulation only during the spin-lock period with long inter-stimulus interval (ISI = 15 s), we investigated the possibility of detecting ncMRI signal in rats without BOLD contamination. In somatosensory cortex of rat, impulse response for BOLD appears with a lag of about 1.5 s, and peaks with a lag of around 2.5 s, then slowly decreases until it disappears after about 7 s (Silva et al., 2007). The BOLD signals evoked by a 1 s train of optical stimulation were obtained with delays on a similar time scale (Kahn et al., 2011). In this study, the spin-lock duration was 70 or 75 ms for SLOE sequence and 130 or 125 ms for SIRS sequence, and optical stimulations (4 ms 100 Hz or 5 ms 40 Hz) were only applied within these durations ($\ll$1 s). With a long inter-stimulus interval (ISI) of 15 s, the ncMRI and BOLD signals could not overlap in the temporal domain.

2. Materials and methods

2.1. Phantom

The phantom used in this study is similar to the design described in Jiang et al. (2015). It consisted of a single copper loop (diameter, 1.1 cm) immersed in a 3.0 mM $NiCl_2$ solution. A Micro 1401 function generator (Cambridge Electronic Design) was connected to produce sinusoidal currents with amplitudes of 0.5 nT at the center of the loop according to the Biot-Savart law for the SLOE experiment and 5 nT for the SIRS experiment. Transistor-transistor logic (TTL) pulses from another channel of the same function generator were generated to trigger an MRI scan every TR and align the sinusoidal currents with the spin-lock module. The loop was positioned perpendicular to the B_0 direction so that the oscillatory magnetic field generated was parallel to B_0. Without BOLD contamination, ISI of 2 s was adopted (T_{SL} current on, 2 sec − T_{SL} current off). For the SLOE experiment, sinusoidal currents with a frequency (f_{curr}) equal to f_{SL} was inputted with initial phases of 0° and 180° alternately (T_{SL} in 1st TR, current on with initial phase = 0°; 2 s – T_{SL}, current off; T_{SL} in 3rd TR, current on with initial phase = 180°, 2 s – T_{SL}, current off) (Fig. 1A). For the SIRS experiment, an oscillatory magnetic field with any initial phase will cause a signal decrease. Thus on-resonance ($f_{curr} = f_{SL} = 100$ Hz) and off-resonance ($f_{curr} = 77$ Hz, $f_{SL} = 100$ Hz) sinusoidal currents were applied alternately with the same initial phase of 0° (Fig. 1C).

2.2. Animals

All animal experiments were performed on male Sprague–Dawley rats in accordance with the protocols approved by the Ethics Committee for Animal Research, Peking University. Electrophysiological recording and MRI data collection were performed on separate animals. Twelve rats were used in the LFP experiment and ten rats were used in the ncMRI experiment.

2.3. Animal surgery

Male Sprague–Dawley rats (200–250 g) were given chloralic hydras injections (400 mg/kg) for anesthesia and then viral injections. The top of the rats' heads were shaved, cleaned with betadine and 70% ethanol, and their eyes were applied with ophthalmic ointment. A small craniotomy was drilled through the skull and 1 μl virus of AAV5-Syn-ChR2 (ET/TC)-EYFP was injected into M1 (2.7 mm AP, 3.0 mm ML, −1.7 mm DV) or V1 cortex (−7.0 mm AP, 3.0 mm ML, −1.15 mm DV). The injection was pushed in using a 10 μl Hamilton syringe with a thin metal needle at a flow rate of 80 nl/min. Two control rats were injected with 1 μl AAV5-Syn-EGFP into M1 cortex in the same manner. After injections, needles were left in place for an additional 10 min and then slowly removed. The cuts were subsequently sutured and cleaned with betadine and 70% ethanol.

After more than 7 weeks for viral expression, the expression of ChR2 was strong enough (Diester et al., 2011) for electrophysiological recording and MRI data collection. A small craniotomy was drilled at the same

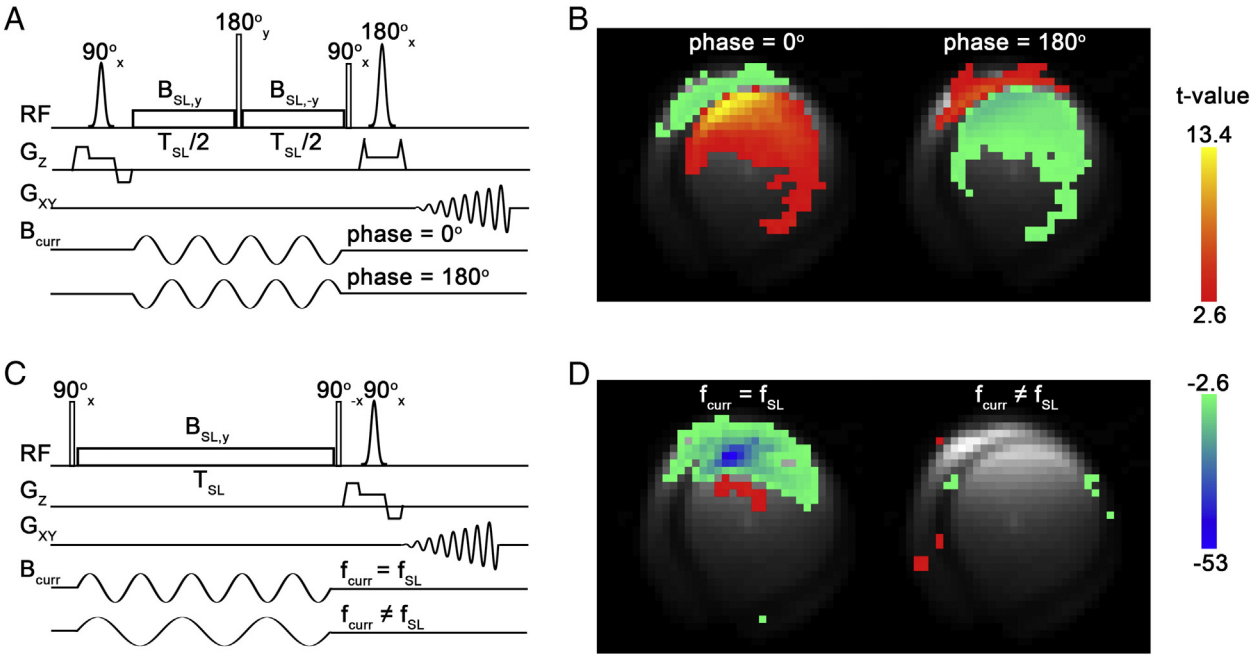

Fig. 1. Timing diagrams of SLOE and SIRS pulse sequences and their corresponding activation t-maps in phantom. (A) SLOE: Sinusoidal current with an amplitude of 0.5 nT and a frequency of 100 Hz ($= f_{SL}$) was inputted with initial phases of 0° and 180° alternately (T_{SL} in 1st TR, current on with phase = 0°; 2 s − T_{SL}, current off; T_{SL} in 3rd TR, current on with phase = 180°, 2 s − T_{SL}, current off). (B) Positive signal changes inside the loop were detected for the set of phase = 0° and negative signal changes were detected inside the loop for the set of phase = 180° using SLOE sequence. The sign of signal change outside the loop was opposite to that inside the loop. (C) SIRS: Sinusoidal currents with an amplitude of 5 nT and an initial phase of 0° were inputted at on-resonance ($f_{curr} = f_{SL} = 100$ Hz) and off-resonance ($f_{curr} = 77$ Hz, $f_{SL} = 100$ Hz) frequencies alternately. (D) Only negative signal changes were detected for the on-resonance condition and no significant signal changes were detected for the off-resonance condition using SIRS sequence.

site of the viral injection. For electrophysiological recording, dura was opened to allow the positioning of an optical fiber and a recording electrode. For MRI acquisition, an MRI compatible cannula (purchased from Plastic One) was inserted through the craniotomy and placed just above the cortex. After that, dental cement was used to fix the cannula to the exposed skull. After the dental cement dried a dummy cap was inserted to cover the cannula.

2.4. Optical stimulation and visual stimulation

Optical stimulations were generated by a 473 nm laser and a 589 nm laser (Changchun New Industries). In the MRI experiment, optical stimulation was delivered via a 500 um unjacketed fiber with a numeric aperture (NA) of 0.5 and the power was less than 16.7 mW (corresponding to 85 mW/mm^2) at the fiber tip. The fiber tip was placed just above the cortex through the cannula. For the part of BOLD MRI, a blocked design (2 ms / 5 ms, 20 Hz) was used. For the part of ncMRI, an event-related design with optical stimulation (4 ms, 100 Hz; 5 ms, 40 Hz) only during the spin-lock period was used.

In the electrophysiological experiment, optical stimulation was delivered via a 300 um unjacketed fiber with NA = 0.37. The fiber tip was positioned 0.5 mm above the cortex with a power of less than 30.6 mW, resulting in a light irradiance of less than 85 mW/mm^2 reaching the cortex surface.

Visual stimulus was generated by a white LED placed 0.5 cm from the contralateral eye. Optical stimulus of 10 ms blue light and visual stimulus of 100 ms were delivered alternately every 30 s for the comparison of their corresponding LFP signals. All light pulses and optical stimulations described in this manuscript referred to optogeneticallly optical stimulation.

2.5. LFP signal recording and analysis

LFP recording was performed in rats with ChR2 expression in V1 cortex. Rats were anesthetized with 1.5–2% isoflurane and 100% O_2. The virus injection site was also used for the optical stimulation and LFP recording. To avoid electrical artifacts, glass electrodes were used and an opaque coating was added to block light transmission to the silver wire (Cardin et al., 2010). The glass was filled with saline (< 1 *MΩ*) and coupled to a direct-current amplifier (MultiClamp 700B, Molecular Device). LFP was recorded in DC mode after the electrodes were inserted into cortex to a depth of about 400–500 μm. For LFP signals recorded in the comparison experiment of the optogenetically versus visually evoked potentials and in the experiment of optogenetically evoked oscillatory potentials, the data was only low-pass filtered at 300 Hz with single-pole RC (Clampfit, Molecular Device). The LFP signals recorded in the rest experiments were band-pass filtered at a range of 1–300 Hz. All the filtered signals were averaged to obtain the mean time course. Spectrogram analysis was further performed on the averaged oscillatory LFP signals.

The inter-stimulus interval (ISI) for the event-related stimulation paradigm in the LFP experiment was 12 s. For LFP adaptation studies and stimulation of pulse series, the time interval was 30 s to ensure that there was no neuronal adaptation caused by repeated stimulations. Please note that the ISIs described here were only adopted in the LFP experiment and were not used in the ncMRI experiment.

2.6. MRI acquisition

Images were acquired using a Bruker Biospec 7.0 T / 20 cm with a body coil to transmit RF power and a single loop surface coil (diameter, 1 cm) to receive RF signal (Bruker, Karlsruhe, Germany). Rats were anesthetized in a knockdown box for 5 min with 4% isoflurane and fixed to the animal bed with tooth and ear bars, then ventilated with 1.5–2% isoflurane and 100% O_2. Breathing rate was monitored continuously (Small Animal Monitoring Model 1025, SA Instruments). With the usual position of the rat's head-tail direction parallel to B_0 in a MRI cradle, the surfaces of M1 and V1 cortex were almost perpendicular to B_0. Since the apical dendrites of pyramidal neurons are approximately perpendicular to cortical surfaces, the neuronal currents were almost

perpendicular to B_0, and thus the B_0 direction component of the resulting neuronal magnetic field would be the strongest.

First a high-resolution T_2-weighted anatomical image was acquired to determine the location of the axial slice containing the fiber tip (copper loop for phantom), where slices of all other scans were centered. It was achieved with a turbo rapid acquisition with relaxation enhancement (turbo RARE) sequence using the following parameters: TE = 33 ms, TR = 2.5 s, RARE factor = 8, slice thickness = 1 mm, FOV = 3 × 3 cm^2 and matrix size = 256 × 256. Then BOLD signal was acquired before and after the whole ncMRI acquisitions to confirm the existence of neuronal response throughout the ncMRI experiment, using a GE-EPI sequence with TE = 25 ms, TR = 1 s, flip angle = 55° (Ernst angle), FOV = 3 × 3 cm^2, matrix size = 64 × 64 and slice thickness = 1 mm.

According to the methods described previously (Borthakur et al., 2004; Wheaton et al., 2004), the longitudinal and transverse relaxation times in the rotating frame $T_{1\rho}$ and $T_{2\rho}$ of rat cortex were measured to be about 60 ms and 84 ms, respectively, and the values were almost the same for both f_{SL} = 40 Hz and 100 Hz. Through simulation of the Bloch equation (Halpern-Manners, 2011; Nagahara and Kobayashi, 2013), T_{SL} equal to 72 ms for SLOE and 135 ms for SIRS were optimum to achieve the maximum contrast. Hence, ncMRI signals were acquired using sequences with the following parameters: 1. SLOE sequence with T_{SL} = 70 ms, f_{SL} = 100 Hz and T_{SL} = 75 ms, f_{SL} = 40 Hz; 2. SIRS sequence with T_{SL} = 130 ms, f_{SL} = 100 Hz and T_{SL} = 125 ms, f_{SL} = 40 Hz. The sequences are illustrated in Fig. 1A and C. Instead of a single hard 90^0 pulse at the start of the spin-lock module, spoiled gradient and selective excitation were used in SLOE sequence and showed more homogenous and stable images. As SLOE method is more sensitive to the main field inhomogeneity (ΔB_0) and incorrect RF power (ΔB_1), a spin-lock module insensitive to ΔB_0 and ΔB_1 was used (Witschey et al., 2007). The TEs for SLOE and SIRS sequences were 5.07 ms and 1.64 ms, respectively, which were the minimum values allowed, and TR = 1 s for both sequences.

For phantom studies, SLOE and SIRS sequences with same parameters as above were used.

2.7. MRI data analysis

Before analyzing the data, the first 10 images of each run were discarded to ensure that MRI signal reached a steady state. 2D motion correction was performed with SPM8. Magnitude signals at each voxel were high-pass filtered with a cutoff of 0.006 Hz to remove slow temporal drift. The residual time series were subsequently analyzed as follows.

BOLD signal was analyzed first to confirm the existence of neuronal response throughout the whole ncMRI experiment. BOLD t-maps were generated by applying the general linear model (GLM) fitted analysis. BOLD and noise regressors were constructed in the same way as ncMRI analysis below. Activated foci were identified with a 2D cluster analysis method (Xiong et al., 1995) with $p < 0.05$ to correct family wise error.

For ncMRI data, GLM fitted analysis (uncorrected, $p < 0.01$) with the following regressors was performed. (1) Neuronal current (nc) regressor: As the electrical signal appears immediately after stimulation, impulse response at every 15 TRs (ISI = 15 TRs) constructs the nc regressor. (2) BOLD regressor: The hemodynamic response function of rat (Schulz et al., 2012; Silva et al., 2007) convolved with the impulse was considered the BOLD regressor. (3) Noise regressors: In order to reveal the comparatively weak ncMRI signal, physiological noise must be considered. Since the area of both ncMRI and BOLD activations were localized, general signal changes of the whole brain area reflect unwanted fluctuation. So the time course of the mean signals across the brain area, which was determined by thresholding all voxels in the first image of every run with an intensity greater than the mean intensity of the image, was used as one of the noise regressors. Additionally, as the phase changing of k-space center point closely follows the respiratory course of the subject (Pfeuffer et al., 2002), its phase evolution also formed one of the noise regressors. Finally, motion parameters were included to construct the noise regressors.

2.8. Histology

To verify ChR2 expression (EGFP expression for control rats), rats were transcardially perfused with saline followed by 4% paraformaldehyde in 100 mM phosphate buffer. Brains were postfixed overnight at 4 °C and then equilibrated in 30% sucrose for at least 24 h before sectioning. 40 μm thick coronal sections were cut on a freezing microtome. For 3 rats with ChR2 injection in V1 cortex, the sections were further stained with DAPI and NeuN. Confocal fluorescence images were acquired on a scanning laser microscope (Leica, Germany).

3. Results

3.1. Phantom

Phantom results shown here were achieved with f_{SL} = 100 Hz, and the results for f_{SL} = 40 Hz were similar. Fig. 1 shows the timing diagrams of SLOE and SIRS sequences and their corresponding phantom results. Activation t-maps in color (uncorrected, $p < 0.01$) were overlaid on the same SIRS image. Using SLOE sequence, positive signal changes were detected inside the loop for the set of phase = 0° and negative signal changes were detected inside the loop for the set of phase = 180° (Fig. 1B). The sign of signal change outside the loop was opposite to that inside the loop due to the opposite sign of the induced magnetic field. This result agrees well with the fact that SLOE method is sensitive to the initial phase of oscillatory current. Using SIRS sequence, however, only negative signal changes were detected for the on-resonance condition and no significant signal change was detected for the off-resonance condition (Fig. 1D).

Fig. 2 shows the mean intensity inside the ROI averaged over 58 trials. The ROI was selected to cover most of the activated voxels inside the loop obtained with SLOE method. For SLOE method, the noise level (standard deviation) was in the range of 0.59%–0.71%, while the mean signal change at the first and third data points (current-on state) relative to the second and fourth data points (current-off state) was 0.96%, which was above the noise level. For SIRS method, the noise level (standard deviation) was in the range of 0.30%–0.36%, while the mean signal change at the first data point (current-on and on-resonance state) relative to the second and fourth data points (current-off state) was 0.47%, which was also above the noise level. Therefore sinusoidal magnetic field with amplitudes of 0.5 nT and

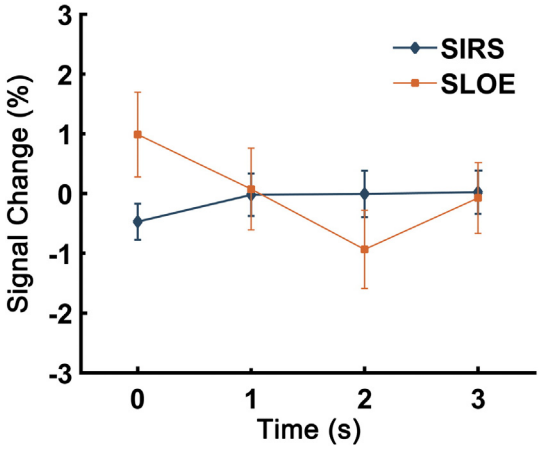

Fig. 2. The ROI-averaged ncMRI signals averaged over 58 trials in phantom experiment. The ROI was selected to cover most activated voxels inside the loop achieved by SLOE acquisition. Error bar indicates ± standard deviation.

5 nT can be robustly detected using SLOE and SIRS methods, respectively. In addition, the noise level of SLOE method is nearly 2-fold larger than SIRS method. The baseline signal of SLOE method is formed by the residual transverse magnetization due to the inhomogeneity of the main magnetic field (B_0) and RF power (B_1). The instabilities of B_0 and B_1 across acquisition time cause a more serious problem in SLOE method than SIRS method.

3.2. LFP

The expressions of ChR2-EYFP (enhanced yellow fluorescent protein) were verified with confocal images for all rats used in this study and Fig. 3A shows a typical example. Overlaying ChR2 with NeuN (red marker) and DAPI (blue marker) reveals ChR2 expression in neuron cells (Fig. 3B, arrow indications). To verify that our LFP recordings were clear of electrical artifacts, we recorded LFP signals induced by paired stimuli of 500 ms blue light and 500 ms yellow light with ISI = 15 s in 3 rats. No signal change was observed for yellow light while blue light induced significant LFP responses (Fig. 3C). This result demonstrates that our LFP signals were recorded without contaminations of electrical artifacts. Fig. 3D shows that the peak amplitudes of LFP signals induced by a 10 ms blue light pulse were significantly larger in rats of 7–8 weeks post-injection than 3–4 weeks post-injection. This is in agreement with the fluorescence intensity course of viral expression in rat cortex (Diester et al., 2011). After about 7 weeks, ChR2 expression reaches a stable maximum so all other experiments in this study used rats which were 7–8 weeks post-injection. Fig. 3E shows neuronal adaption in the LFP signals to 500 ms blue light pulses (n = 4). For ISI = 12 s, the LFP signal was already consistent in all trials. Hence no neuronal adaptation could occur during ncMRI experiments with optical stimulation delivered at ISI = 15 s.

Fig. 3F shows the LFP signals induced by paired stimuli of 10 ms optical blue light and 100 ms visual stimulus (white LED). While visually evoked potential (VEP) signal changes were delayed by several tens of milliseconds after visual stimulus, optogenetically evoked potential (OEP) signal changes appeared immediately after optical stimulus. To capture maximum neuronal electrical activity, a time delay of various values for different subjects was needed between the start of visual stimulation and ncMRI data acquisition (Luo et al., 2009, 2011). However, for optical stimulus, no time delay was needed and it was convenient to align optogenetically evoked neuronal electrical activity with the spin-lock module at millisecond accuracy.

Stimulated with a series of 5 ms pulses at different rates (20 Hz, 50 Hz, 80 Hz), oscillatory LFP signals were induced with their main spectral components located at the frequencies equal to the stimulation rates (Fig. 4). The amplitudes of the main spectral components went smaller (80Hz's < 50Hz's < 20Hz's) as frequencies of the stimulus increased. However, the sensitivity of SLOE method would decrease with lower spin-lock RF intensity (B_{SL}) because of the inhomogeneities of B_0 and B_1 fields (Jiang et al., 2015). If ΔB_0 is comparable to B_{SL} and cannot be neglected any more, the intensity of the effective spin-lock field would become $\sqrt{\Delta B_0{}^2 + B_{SL}{}^2}$ and the effective spin-lock direction would deviate from the original spin-lock direction by an angle of $\arctan(\frac{\Delta B_0}{B_{SL}})$. Therefore we chose both high and low spin-lock frequencies (100 Hz and 40 Hz) in the ncMRI experiment design. Although we didn't record LFP data for 40 Hz or 100 Hz, our results here and similar LFP signals evoked by 20–150 Hz stimulation in the study of Diester et al. (2011) both support the fact that optogenetically evoked LFP signals change with the stimulation frequency, and its main spectral component would locate at the stimulation frequency. Previous studies across motor cortex, posterior parietal cortex, somatosensory cortex and medial septal have shown similar conclusions (Diester et al.,

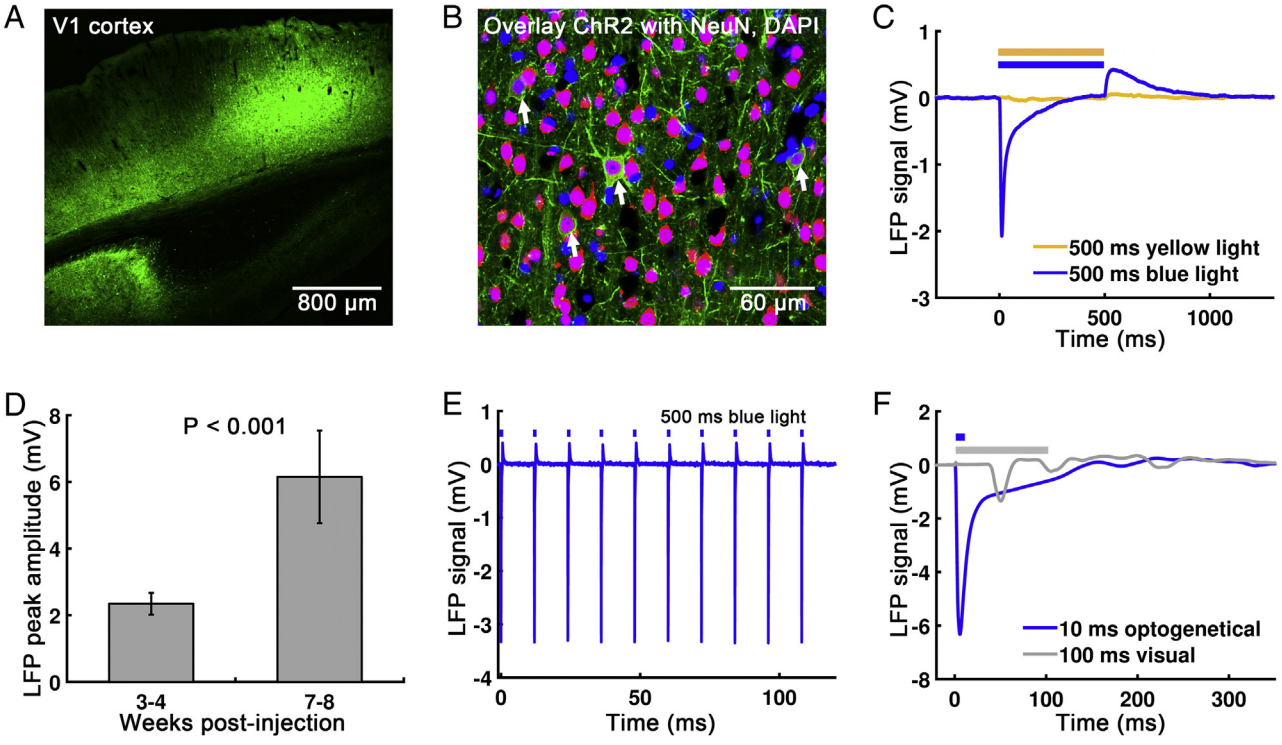

Fig. 3. ChR2 expression and optogenetically evoked LFP signals in V1 cortex of rats. (A) ChR2 expression in V1 cortex of one typical rat. (B) The arrows indicate ChR2 expression in neuron cells. (C) Optogenetical LFP signals induced by paired stimuli of 500 ms blue light and 500 ms yellow light (n = 3). (D) The peak amplitudes of LFP induced by 10 ms blue light pulse in rats 7–8 weeks post-injection were significantly larger than that induced in rats 3–4 weeks post-injection. (E) Neuronal adaptation in the LFP signals to 500 ms blue light pulses (n = 4). For ISI = 12 s, the LFP responses are already consistent for all pulses. (F) LFP signals induced by optical stimulus of 10 ms blue light and visual stimulus of 100 ms (white LED) in one typical rat. The blue and yellow bars stand for the optical stimuli of blue and yellow light, respectively, while the gray bar stands for visual stimulus. The virus injection site was also used as the optical stimulation site and LFP recording point.

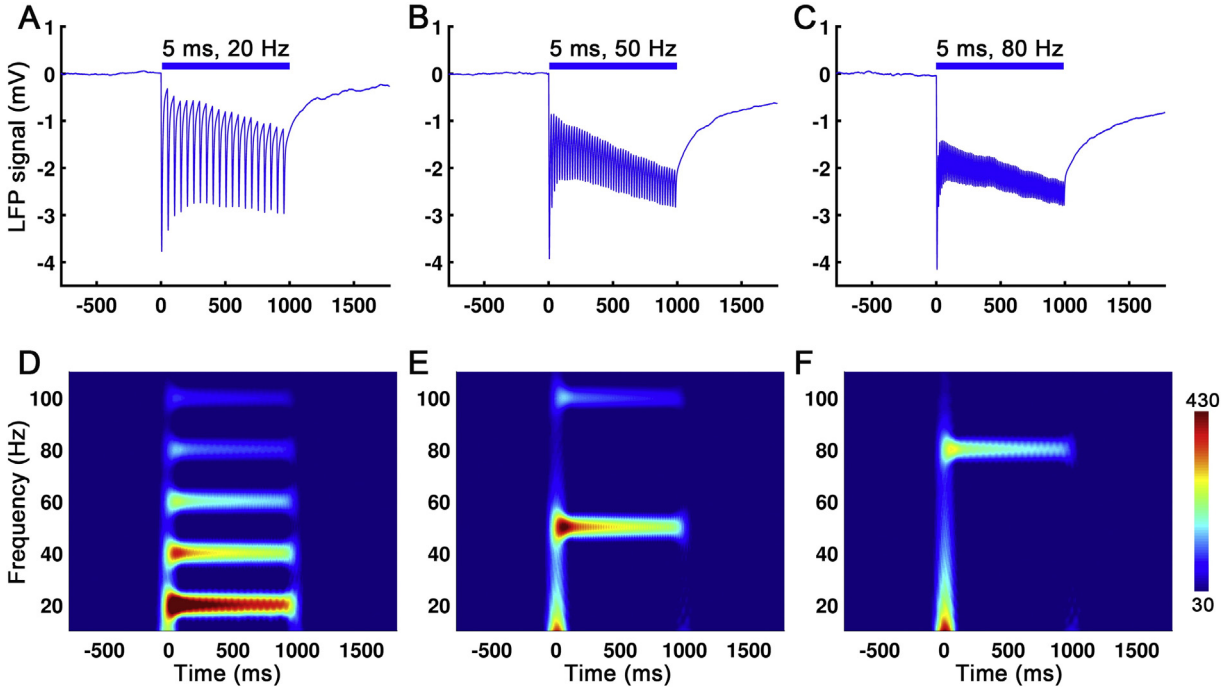

Fig. 4. Optogenetically evoked oscillatory LFP signals (A–C) and their corresponding spectrograms (D–F). The blue bars stand for optical stimuli of blue light. The virus injection sites in V1 cortex were also used as the optical stimulation sites and LFP recording points.

2011; Jing et al., 2012; Kahn et al., 2011; Laxpati et al., 2014). Since the optogenetically evoked potential is induced by ion flow through ChR2 channel, the feature of LFP signal locking to the stimulus frequency is in accordance with the pulse stimulated ChR2 photocurrent (Grossman et al., 2013).

3.3. BOLD

In all eight rats with ChR2 intensely expressed (six rats in M1 cortex, two rats in V1 cortex), robust BOLD signals were detected before and after the whole ncMRI acquisitions to confirm the existence of neuronal response throughout ncMRI experiment. BOLD t-maps obtained after the whole ncMRI acquisitions from one rat with ChR2 expression in M1 cortex and another rat with ChR2 expression in V1 cortex are shown in Fig. 5A and C, respectively. Significant BOLD signals were detected from the area below the fiber tip, and the related time course of the signals from positively activated regions corresponded well with the optical stimuli (Fig. 5B and D). Fig. 5E shows a typical example of control rats injected with AAV5-Syn-EGFP, no significant positive BOLD signal with good responding time course (Fig. 5F) was detected from the area below fiber tip. The resulted activity map differs significantly from those of ChR2-expressing rats. However, some negative signal changes were occasionally detected from the area just below the fiber tip in both control and ChR2-expressing rats. These signals are believed to be resulting from heating effects (Christie et al., 2013). Supplementary Fig. S1 shows that in one rat with ChR2 expression in M1 cortex, both blue and yellow optical stimulations could induce negative signal changes from the area below fiber tip, but only blue optical stimulation could induce a positive BOLD signal change.

3.4. ncMRI

Figs. 6 and 7 show the ncMRI activation t-maps from two rats: one with ChR2 expression in M1 cortex (ChR2-M1 rat), and another with ChR2 expression in V1 cortex (ChR2-V1 rat). The spin-lock RF intensity used here was 100 Hz for both SLOE and SIRS experiments. The experiments of spin-lock RF intensity at 40 Hz obtained similar results but were not shown here. To avoid confounders from heating effects of optical stimuli, the alternating stimulation pattern same as the phantom experiment were adopted with ISI = 15 s. While ncMRI signals are sensitive to the initial phase (using SLOE) and on (off) -resonance frequencies (using SIRS) of oscillatory neuronal electrical activity, heating effects are not sensitive to either of them.

Fig. 6A shows the timing diagrams of optical stimulation and ncMRI acquisition using SLOE sequence. Optical stimulus 1 (stim1) and stimulus 2 (stim2) were applied alternately every 15 s (T_{SL} stim1, 15 sec − T_{SL} off, T_{SL} stim2, 15 sec − T_{SL} off). The onset of stim1 was synchronized with the start of the spin-lock RF pulse whereas the first pulse of stim2 began half a pulse interval in advance. In this way, oscillatory electrical signal of opposite initial phases, analogous to Fig. 1A, could be induced. Fig. 6B shows the activation t-maps of the ChR2-M1 rat using SLOE sequence. No significant ncMRI signal change of opposite signs in the area below fiber tip were detected for stim1 or stim2. Since stim1 and stim2 owned almost the same total time, they were treated as the same stimulus for the BOLD detection. Although the optical stimulus was weak and SLOE method was expected to be insensitive to BOLD signals (Jiang et al., 2015), BOLD activation (uncorrected, $p < 0.01$) was in fact observed. Fig. 6C shows activation t-maps from the ChR2-V1 rat using SLOE sequence, which shows similar features as Fig. 6B.

Fig. 7A shows the timing diagrams of optical stimulation and ncMRI acquisition using SIRS sequence. Optical stimulus 1 (stim1) and stimulus 2 (stim2) were also performed alternately every 15 s. The onsets of both stim1 and stim2 were synchronized with the start of the spin-lock RF pulse. The frequency of stim1 was on resonance with the spin-lock RF field ($f_{stim1} = f_{SL}$) while the frequency of stim2 was not ($f_{stim2} \neq f_{SL}$). In this way, oscillatory electrical activity on-resonance and off-resonance with spin-lock field, analogous to Fig. 1C, could be induced. Fig. 7B shows ncMRI t-maps from the ChR2-M1 rat using the SIRS sequence. No significant ncMRI signal change in the area below fiber tip was found for stim1, apart from several scattered points. For the control condition of stim2, activations were only observed at scattered points. Although different stimulation frequencies were applied, the total time of optical stimulation is same for stim1 and stim2. Therefore the

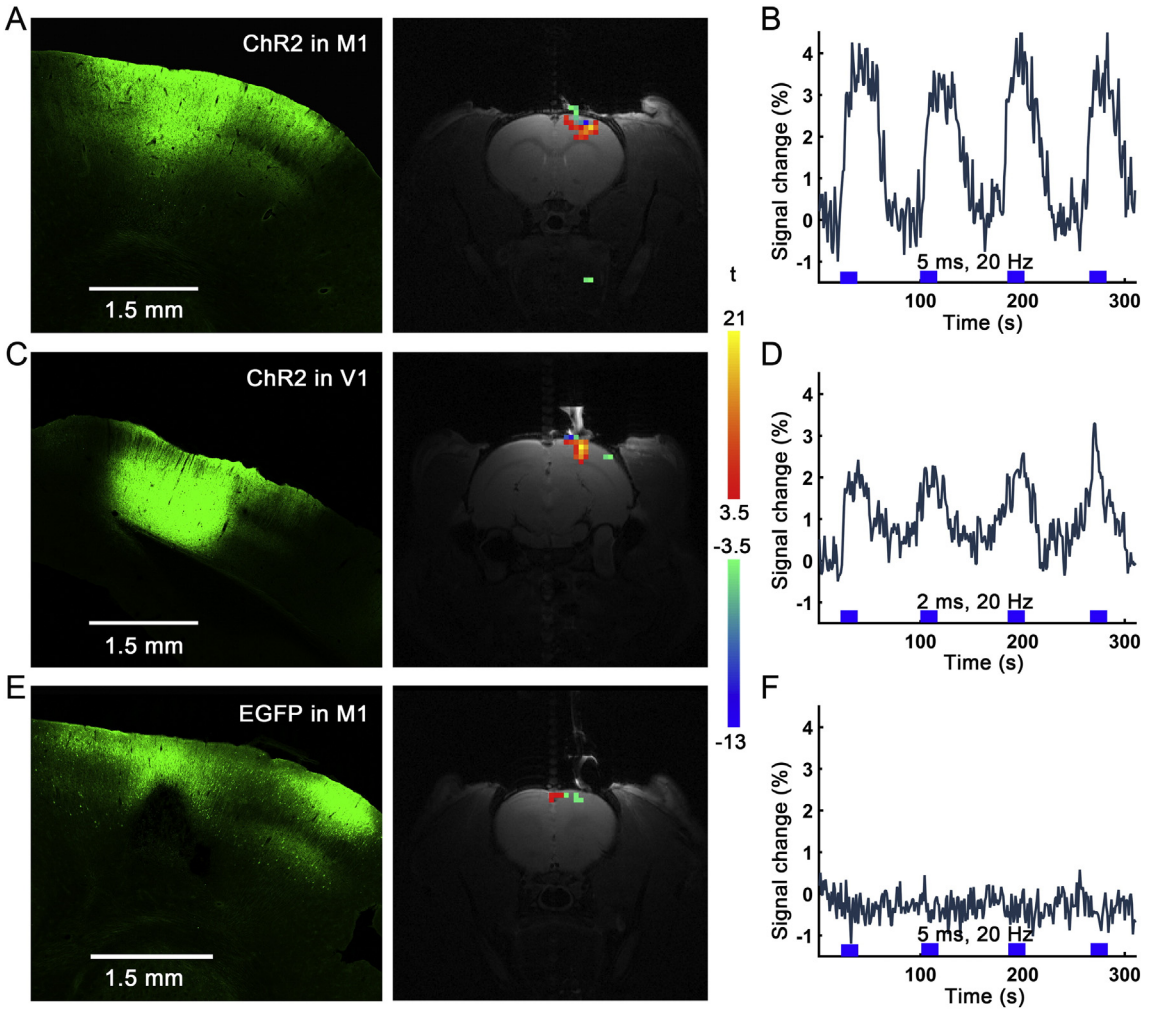

Fig. 5. BOLD signals acquired after whole ncMRI acquisition. (A) BOLD t-map in one rat with ChR2 expression in M1 cortex and (B) its ROI-averaged time course. (C) BOLD t-map in one rat with ChR2 expression in V1 cortex and (D) its ROI-averaged time course. (E) BOLD t-map in one control rat with EGFP expression in M1 cortex and (F) its ROI-averaged time course. The ROIs were selected to cover most of the positive BOLD activated voxels for ChR2 rats and the similar area below fiber tip for the control rat. The blue bars stand for optical stimuli of blue light. The optical stimulation sites were at the same sites of virus injection.

BOLD responses and possible heating effects induced by stim1 and stim2 were the same. Consistently with the SLOE results, BOLD signals were also detected. Fig. 7C shows ncMRI t-maps of the ChR2-V1 rat using SIRS sequence. There was significant positive ncMRI signal change in the area below fiber tip for both stim1 and stim2. However, given the off-resonance condition of stim2, there should not be any ncMRI signal change for stim2. In addition, the sign of ncMRI signal change was not in accordance with heating effects (see Fig. 9). Thus these signal changes were not resulting from ncMRI effects or heating effects. This circumstance might have been caused by physiological noise and was not observed in other ChR2 rats. The BOLD result was similar to that of the ChR2-M1 rat.

The same ncMRI data of Figs. 6 and 7 was also analyzed in a ROI fashion. The ROI was selected to cover most BOLD activated voxels achieved by GE-EPI acquisition as Fig. 5. The mean intensity inside the ROI was averaged over 80 trials. This analysis was applied to the ncMRI data of all eight rats (six rats in M1 cortex, two rats in V1 cortex). Then, the averaged time courses and standard deviations from every rat were averaged to get Fig. 8. So the standard deviation in Fig. 8 reflects the mean noise level across all eight rats. For SLOE method, the mean noise level (standard deviation) was in the range of 1.20%–1.40%, which was 2-fold larger than that in phantom study. For SIRS method, the noise level was in the range of 1.60%–1.79%, which was about 5-fold larger than that in phantom study. There are two reasons for the increasing noise level. First, the scanning time was 40 min for rat study, while it was only 4 min for phantom study. Second, physiological noise in vivo increased the noise level. In contrast to a higher noise level of SLOE method than SIRS method in phantom study, in vivo result shows a similar or even higher noise level in SIRS method than SLOE method. This indicates that SLOE method is less sensitive to physiological noise than SIRS method, which agrees with a previous prediction (Jiang et al., 2015). The increasing noise level in vivo will deteriorate signal stability and lead to a poor sensitivity.

Fig. 9 shows timing diagrams of the control experiment and ncMRI artifacts detected in a control rat injected with AAV5-Syn-EGFP. In order to induce detectable heating artifacts, continuous stimulation during the spin-lock period at 2-fold power (2×80 mW/mm^2) was adopted, and the fiber tip was inserted into the cortex. Fig. 9B shows that only negative ncMRI artifacts were detected from the area below the fiber tip using both SLOE and SIRS sequences. Although these artifacts could not be observed with the ncMRI design at the normal power (85 mW/mm^2) adopted by Figs. 6A and 7A, they did exist and might have contaminated the real ncMRI signals. Hence an alternating stimulation pattern was adopted in the ncMRI design. While the heating effects induced by stim1 and stim2 (Figs. 6A and 7A) were almost the same, the induced ncMRI signal changes were expected to be quite different.

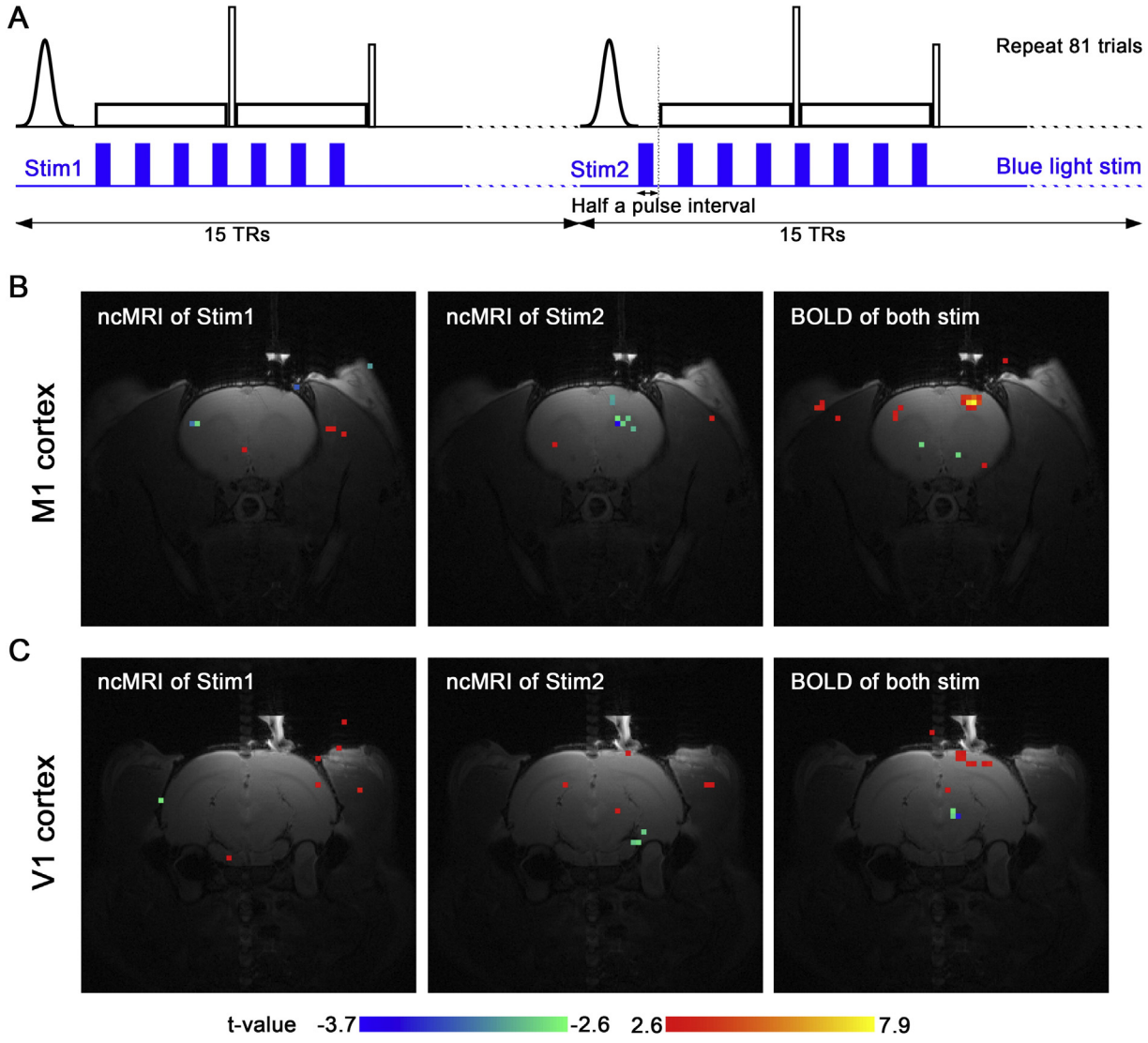

Fig. 6. Timing diagrams of the ncMRI experiment design using SLOE sequence and its activation t-maps. (A) Optical stimulus 1 (stim1) and stimulus 2 (stim2) were applied alternately every 15 s. 4 ms/100 Hz was used for both stims and every blue bar stands for a single pulse of 4 ms. The onset of stim1 was synchronized with the spin-lock RF pulse whereas the first pulse of stim2 began half a pulse interval in advance. (B) Activation t-maps from one rat with ChR2 expression in M1 cortex. No significant ncMRI signals of opposite signs were detected for stim1 and stim2, respectively, in the area below fiber tip. Only BOLD signals were detected. (C) Activation t-maps from one rat with ChR2 expression in V1 cortex. The virus injection sites were also used as optical stimulation sites.

4. Discussion

In this study, SLOE and SIRS sequences were used in vivo for the first time to directly detect oscillatory neuronal electrical activity evoked by optogenetic techniques in rats. Although clear oscillatory LFP signals and intense BOLD signals were acquired in the area of ChR2 expression and optical stimulation, no significant ncMRI signal change was detected using either spin-lock sequence. These results are ascribed to the following questions.

4.1. Are oscillatory LFP signals always accompanied with a similar spectrally distributed oscillatory magnetic field?

Evoked by optogenetic techniques in rats, oscillatory LFP signals, whose main spectral component can be manipulated artificially to match the resonance frequency of spin-lock RF field, were recorded. However spin-lock oscillatory excitation works only if a similar oscillatory magnetic field accompany with oscillatory LFP. In previous work, separate recording of the electrophysiological and magnetic signals evoked by the same stimulus showed similar spectral distributions. Steady-state visually evoked potentials (SSVEPs) observed on both electrophysiological recording (Herrmann, 2001; Rager and Singer, 1998) and computer simulation (Du et al., 2012) showed that LFP or EEG spectrum had peaks at the stimulus frequency and its multiple frequencies. MEG signal recorded in visual cortex also followed the alternating visual stimulus (Bandettini et al., 2005) and showed a similar spectral distribution as electrophysiological signal (Fawcett et al., 2004). Petridou et al. (2006) measured EEG and MR data of organotypic rat brain cultures in vitro before and after the blockade of neuronal activity with tetrodotoxin. A similar spectral pattern and signal power decrease were observed in MR phase and EEG signal. Sundaram et al. (2010) performed MR and EEG measurements of epileptiform spikes concurrently and found a temporal derivative relationship between MR phase and scalp EEG signal, suggesting that the local magnetic field change might be tightly linked to the local cerebral electrical activity. Additionally, the MEG and EEG measurements of alpha activity in a subject relaxed with eyes closed showed activities with a similar spectral pattern of 8–13 Hz in parieto-occipital areas (Hämäläinen et al., 1993).

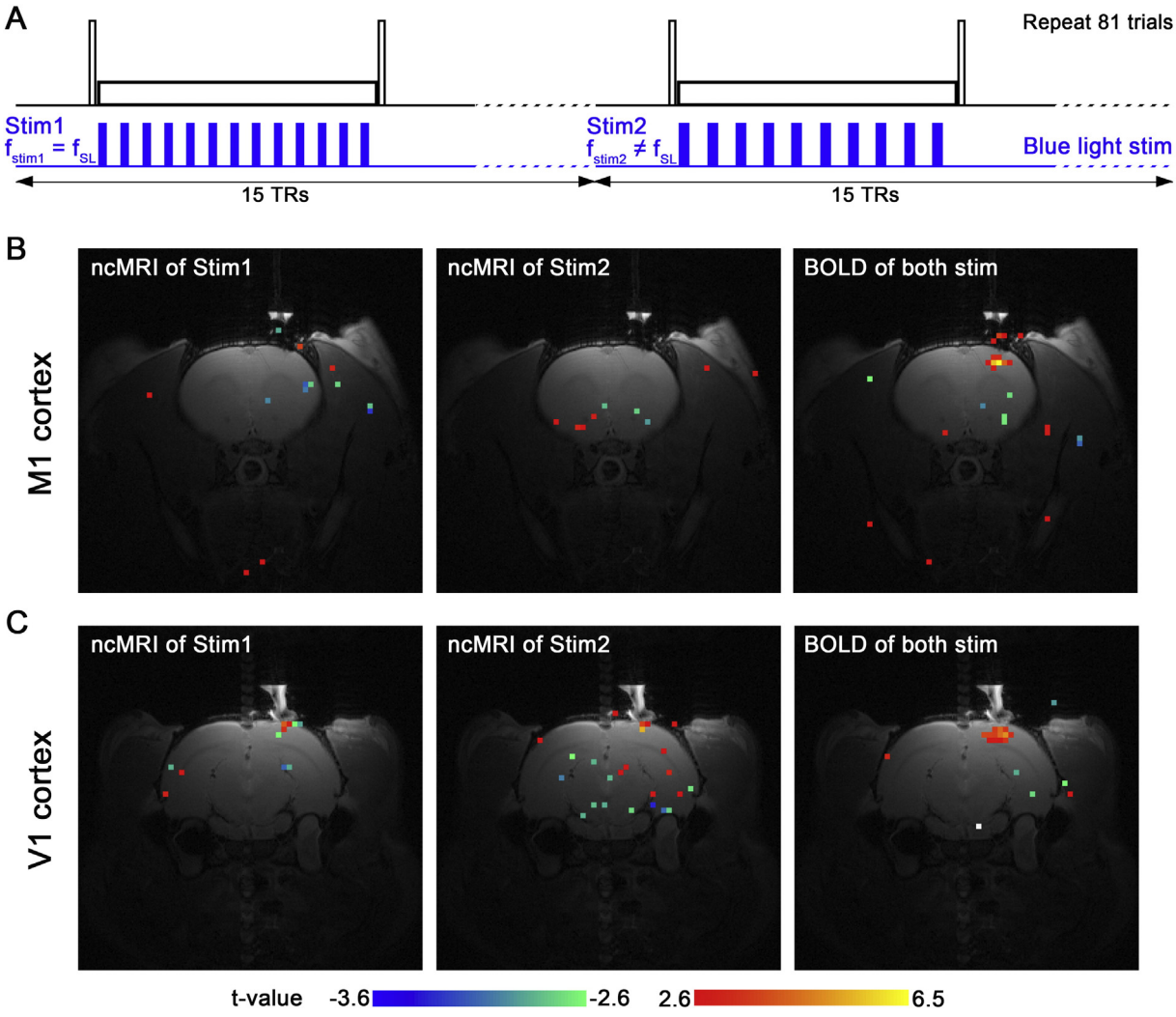

Fig. 7. Timing diagrams of the ncMRI experiment design using SIRS sequence and its activation t-maps. (A) Optical stimulus 1 (stim1, 4 ms/100 Hz) and stimulus 2 (stim2, 5.2 ms/77 Hz) were performed alternately every 15 s. Every single blue bar stands for a single laser pulse. The frequency of stim1 was on resonance with the spin-lock RF field ($f_{stim1} = f_{SL}$), while frequency of stim2 was not ($f_{stim2} \neq f_{SL}$). (B) Activation t-maps from one rat with ChR2 expression in M1 cortex. No significant ncMRI signal changes were detected from the area below the fiber tip for both on- and off-resonance conditions. Only BOLD signal changes were detected. (C) Activation t-maps from one rat with ChR2 expression in V1 cortex. The virus injection sites were also used as the optical stimulation sites.

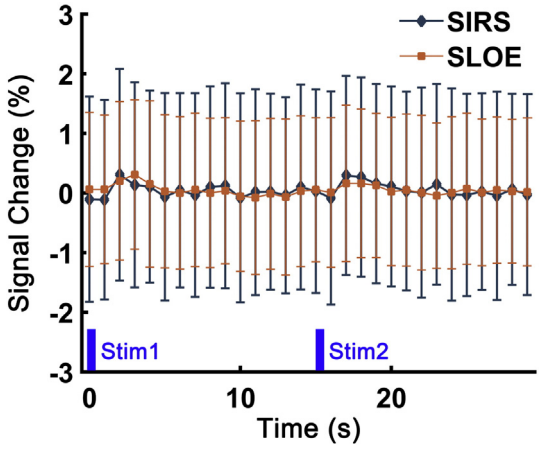

Fig. 8. The mean ROI-averaged ncMRI signals averaged over 80 trials for 8 rats in ncMRI experiment. The data acquisition was same with Figs. 6 and 7, so was the representations of stim1 and stim2. The ROI was selected to cover most BOLD activated voxels achieved by GE-EPI acquisition. Error bar indicates ± standard deviation, which equals to the mean standard deviation for all 8 rats.

4.2. Is spin-lock sequence sensitive enough to detect optogenetically evoked oscillatory neuronal electrical activity?

Based on the imaging parameters used in phantom study, the sensitivities of SLOE and SIRS methods were 0.5 nT and 5 nT, respectively, for a sinusoidal oscillatory electrical activity. However physiological noise and poor inhomogeneity of the main field in vivo would deteriorate signal stability and lead to a decreased sensitivity. In a living system, the sensitivity of applied sinusoidal current decreased to the order of nanotesla for SLOE method (our unpublished data). In addition, the appearance of the optogenetically evoked oscillatory LFP signal was not sinusoidal, neither was the corresponding NMF signal. As FWHM of spin-lock saturation spectra for SLOE method is only 6 Hz (Jiang et al., 2015), the sensitivity to detect physiological electrical activity in vivo would decrease further. On the other hand, no experimental evidence has provided a proper amplitude value for optogenetically evoked magnetic field. Only some estimations were suggested through theoretic models, such as the derivation of ncMRI phase changes in vitro, or the inverse conduction of MEG signals. None of them were specifically designed for oscillatory NMF. For a stimulated activation of the primary visual cortex of cat, NMF of 0.5 nT mainly from postsynaptic activity was

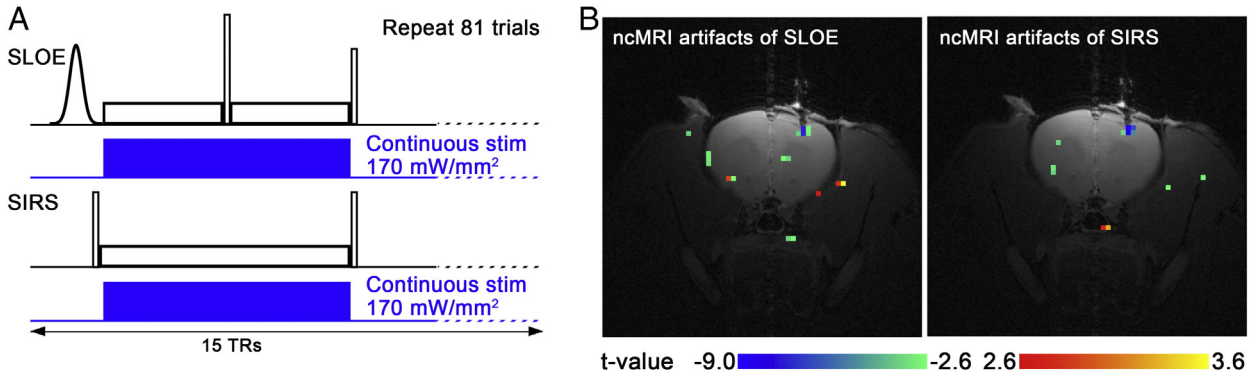

Fig. 9. Timing diagrams of control experiment and ncMRI artifacts detected in a control rat with AAV5-Syn-EGFP expression in M1 cortex. (A) The blue bars stand for continuous optical stimulations during spin-lock period (70 ms for SLOE experiment and 130 ms for SIRS experiment). The stimulation power was 2-fold larger than that in ncMRI experiments of ChR2 rats. (B) Negative ncMRI artifacts were detected from the area below the fiber tip. The virus injection site was also used as the optical stimulation site.

predicted through simulation of laminar cortex model (Du et al., 2014). Petridou et al. (2006) predicted a magnetic field change from 0.2 to 3.9 nT in the organotypic rat brain cultures in vitro before and after the blockade of neuronal activity with tetrodotoxin. According to the 10^{-4}–10^{-3} nT scalp magnetic field measured by MEG, local field change on the order of 0.1–1 nT could be deduced by the inverse scaled factor (Bodurka and Bandettini, 2002). As SLOE and SIRS methods are only sensitive to the resonant spectral components extracted from the original neuronal electrical activity, the effective amplitude of oscillatory magnetic field contributing to rotary saturation would be much smaller than the estimations above.

4.3. Can more neurons be activated synchronously to induce larger neuronal electrical activity?

In ncMRI experiment of this study, the diameter of fiber was 500 um and the cortical depth at which light irradiance decreases to 1 mW/mm^2 is about 1 mm. As fiber NA was 0.5, the stimulation volume was about 1 mm^3, which covered about 4 voxels in ncMRI images. Only neurons in this volume were stimulated directly and neurons outside this region might have been stimulated indirectly through neuronal interaction. If more neurons are expected to be stimulated directly, fibers with larger diameter should be used or the fiber tip should be positioned at some distance above the cortex and larger area of the cortex surface should be exposed. In this way, more neurons could be activated synchronously and this can be explored in future studies. In addition, the upper limit of optical irradiance adopted in this study was 85 mW/mm^2. If the optical irradiance was increased, larger neuronal electrical activity might be induced, but neurons might be damaged and ncMRI artifacts must have been taken into consideration. In this case, imaging the projected regions as oppose to local stimulation regions could be considered, but the feature of the evoked neuronal electrical activity in the projected region must be studied first. Besides, we chose the viral type of AAV5-Syn-ChR2(ET/TC)-EYFP in this study and it produced significant oscillatory neuronal electrical signal for spin-lock oscillatory excitation. Of course there is a possibility that, with the usage of other viral types such as AAV9, higher infection efficiency could be achieved and oscillatory electrical activity with larger main spectral component could be induced.

4.4. Did the BOLD signals, physiological noises, heating artifacts and anesthetized condition confound ncMRI signals in this study?

Although Jiang et al. (2015) predicted that SLOE method should be insensitive to BOLD signals or physiological noises, we did observe significant BOLD signals using SLOE sequence (Fig. 6B and C). Hence we adopted a long ISI to ensure that BOLD signals had returned to their baselines for both spin-lock sequences. To reveal the comparatively weak ncMRI signal, regressors of physiological noises were included in the GLM fitted analysis. They consisted of general signal changes of the whole brain area reflecting unwanted fluctuation, phase change of central k-space point closely following respiratory trajectory, and estimation of motion correction. With optical stimulation, heating effects must be taken into account in optogenetic fMRI experiments (Christie et al., 2013). In control rats with much stronger optical stimulation, ncMRI artifacts of negative signal changes were observed for both spin-lock sequences (Fig. 9B). Although no significant artifact was retained with the ncMRI designs of ChR2-expressing rats, paired stimuli with opposite phases for SLOE, which were expected to induce ncMRI signals of opposite signs, and stimuli with on-resonance and off-resonance frequencies for SIRS, which were expected to induce negative and no ncMRI signals, respectively, were adopted to remove heating confounders. Furthermore, increasing studies have shown that anesthesia can tremendously dampen the opto-fMRI signal (Desai et al., 2011; Liang et al., 2015) and it might have also affected ncMRI signal here. However, the different hemodynamic responses between in awake and anesthetized conditions are more likely to be resulting from a change in neurovascular coupling, and the overall neural response showed much smaller differences for the two conditions (Pisauro et al., 2013).

4.5. Would smaller voxel size provide greater potential for a successful detection of ncMRI signals?

There is no doubt that local NMF exists, and the expected ncMRI signals aim to integrate the local effects on both temporal and spatial domains. As rich temporal information about neuronal activity can be provided by electrophysiological recording techniques, optimal TE for GE-EPI sequence, optimal T_{SL} for spin-lock sequence and proper alignments of the activity duration with acquisition window are all achievable for ncMRI acquisitions. However, no optimal voxel size for ncMRI acquisition has been suggested by any experiment or theoretical study except for some indefinite predictions because there is currently no clear understanding about the spatial distribution of NMF in an activated cortical area. Because the phase signal of GE-EPI sequence is sensitive to the sign of magnetic field, as well as the signal of SLOE sequence to the initial phase of oscillatory magnetic field, the integral signal over a voxel is susceptible to be canceled out. For the GE-EPI sequence mostly used in recent ncMRI studies, Du et al. (2014) studied the effect of voxel size on phase signal change through computer simulation, and found that small voxels are likely to produce large phase change as the peaks and troughs of neuronal magnetic field can only be discerned by employing small voxels. For magnitude signal of GE-EPI sequence and SIRS sequence, although it is insensitive to the intra-voxel cancelations caused by phase of NMF, the partial volume effect is another concern.

If the voxel size is much larger than the activation area, the average signal in a voxel will be diluted thoroughly. Therefore spatial spectrum of the local NMF changes in the activated area needs to be clarified by future studies.

5. Conclusions

In this study, SLOE and SIRS sequences were used to directly detect oscillatory neuronal electrical activity in vivo for the first time. Applying optogenetic techniques in rats, oscillatory LFP signals, whose main spectral component can be manipulated artificially to match the resonance frequency of spin-lock RF field, were induced. To directly detect neuronal electrical activity induced MRI signal changes, further understanding about the local NMF in the activated area and improvement on the sensitivity of SLOE sequence are needed.

Supplementary data to this article can be found online at http://dx.doi.org/10.1016/j.neuroimage.2015.10.058.

Acknowledgments

This work was supported by China's National Strategic Basic Research Program (973) (2012CB720700), the Natural Science Foundation of China (81227003, 81430037, 31421003, 91132307 and 31171061) and the Strategic Priority Research Program of the Chinese Academy of Sciences (XDB02050002).

References

Bandettini, P.A., Petridou, N., Bodurka, J., 2005. Direct detection of neuronal activity with MRI: fantasy, possibility, or reality? Appl. Magn. Reson. 29, 65–88.
Bianciardi, M., Di Russo, F., Aprile, T., Maraviglia, B., Hagberg, G.E., 2004. Combination of BOLD-fMRI and VEP recordings for spin-echo MRI detection of primary magnetic effects caused by neuronal currents. Magn. Reson. Imaging 22, 1429–1440.
Bodurka, J., Bandettini, P.A., 2002. Toward direct mapping of neuronal activity: MRI detection of ultraweak, transient magnetic field changes. Magn. Reson. Med. 47, 1052–1058.
Borthakur, A., Wheaton, A.J., Gougoutas, A.J., Akella, S.V., Regatte, R.R., Charagundla, S.R., Reddy, R., 2004. In vivo measurement of T1rho dispersion in the human brain at 1.5 Tesla. J. Magn. Reson. Imaging 19, 403–409.
Buzsaki, G., Anastassiou, C.A., Koch, C., 2012. The origin of extracellular fields and currents—EEG, ECoG, LFP and spikes. Nat. Rev. Neurosci. 13, 407–420.
Cardin, J.A., Carlen, M., Meletis, K., Knoblich, U., Zhang, F., Deisseroth, K., Tsai, L.H., Moore, C.I., 2010. Targeted optogenetic stimulation and recording of neurons in vivo using cell-type-specific expression of Channelrhodopsin-2. Nat. Protoc. 5, 247–254.
Christie, I.N., Wells, J.A., Southern, P., Marina, N., Kasparov, S., Gourine, A.V., Lythgoe, M.F., 2013. fMRI response to blue light delivery in the naive brain: implications for combined optogenetic fMRI studies. Neuroimage 66, 634–641.
Desai, M., Kahn, I., Knoblich, U., Bernstein, J., Atallah, H., Yang, A., Kopell, N., Buckner, R.L., Graybiel, A.M., Moore, C.I., Boyden, E.S., 2011. Mapping brain networks in awake mice using combined optical neural control and fMRI. J. Neurophysiol. 105, 1393–1405.
Diester, I., Kaufman, M.T., Mogri, M., Pashaie, R., Goo, W., Yizhar, O., Ramakrishnan, C., Deisseroth, K., Shenoy, K.V., 2011. An optogenetic toolbox designed for primates. Nat. Neurosci. 14, 387–397.
Du, J., Vegh, V., Reutens, D.C., 2012. The laminar cortex model: a new continuum cortex model incorporating laminar architecture. PLoS Comput. Biol. 8, e1002733.
Du, J., Vegh, V., Reutens, D.C., 2014. MRI signal phase oscillates with neuronal activity in cerebral cortex: implications for neuronal current imaging. Neuroimage 94, 1–11.
Fawcett, I.P., Barnes, G.R., Hillebrand, A., Singh, K.D., 2004. The temporal frequency tuning of human visual cortex investigated using synthetic aperture magnetometry. Neuroimage 21, 1542–1553.
Grossman, N., Simiaki, V., Martinet, C., Toumazou, C., Schultz, S., Nikolic, K., 2013. The spatial pattern of light determines the kinetics and modulates backpropagation of optogenetic action potentials. J. Comput. Neurosci. 34, 477–488.
Halpern-Manners, N.W., 2011. Applications of Magnetic Resonance to Current Detection and Microscale Flow Imaging.
Hämäläinen, M., Hari, R., Ilmoniemi, R.J., Knuutila, J., Lounasmaa, O.V., 1993. Magnetoencephalography—theory, instrumentation, and applications to noninvasive studies of the working human brain. Rev. Mod. Phys. 65, 413–497.
Herrmann, C.S., 2001. Human EEG responses to 1–100 Hz flicker: resonance phenomena in visual cortex and their potential correlation to cognitive phenomena. Exp. Brain Res. 137, 346–353.
Jiang, X., Sheng, J., Li, H., Chai, Y., Zhou, X., Wu, B., Guo, X., Gao, J.H., 2015. Detection of subnanotesla oscillatory magnetic fields using MRI. Magn. Reson. Med. http://dx.doi.org/10.1002/mrm.25553.
Jing, W., Fabien, W., David, A.B., Jiayi, Z., Ilker, O., Rebecca, D.B., Arto, V.N., Rick van, W., Ilka, D., Karl, D., 2012. Integrated device for combined optical neuromodulation and electrical recording for chronic in vivo applications. J. Neural Eng. 9, 016001.
Kahn, I., Desai, M., Knoblich, U., Bernstein, J., Henninger, M., Graybiel, A.M., Boyden, E.S., Buckner, R.L., Moore, C.I., 2011. Characterization of the functional MRI response temporal linearity via optical control of neocortical pyramidal neurons. J. Neurosci. 31, 15086–15091.
Konn, D., Gowland, P., Bowtell, R., 2003. MRI detection of weak magnetic fields due to an extended current dipole in a conducting sphere: a model for direct detection of neuronal currents in the brain. Magn. Reson. Med. 50, 40–49.
Laxpati, N.G., Mahmoudi, B., Gutekunst, C.-A., Newman, J.P., Zeller-Townson, R.T., Gross, R.E., 2014. Real-time in vivo optogenetic neuromodulation and multielectrode electrophysiologic recording with neurorighter. Front. Neuroeng. 7.
Liang, Z., Watson, G.D., Alloway, K.D., Lee, G., Neuberger, T., Zhang, N., 2015. Mapping the functional network of medial prefrontal cortex by combining optogenetics and fMRI in awake rats. Neuroimage 117, 114–123.
Liston, A.D., Salek-Haddadi, A., Kiebel, S.J., Hamandi, K., Turner, R., Lemieux, L., 2004. The MR detection of neuronal depolarization during 3-Hz spike-and-wave complexes in generalized epilepsy. Magn. Reson. Imaging 22, 1441–1444.
Lopes da Silva, F., 2004. Functional localization of brain sources using EEG and/or MEG data: volume conductor and source models. Magn. Reson. Imaging 22, 1533–1538.
Luo, Q., Lu, H., Lu, H., Senseman, D., Worsley, K., Yang, Y., Gao, J.H., 2009. Physiologically evoked neuronal current MRI in a bloodless turtle brain: detectable or not? Neuroimage 47, 1268–1276.
Luo, Q., Jiang, X., Gao, J.H., 2011. Detection of neuronal current MRI in human without BOLD contamination. Magn. Reson. Med. 66, 492–497.
Nagahara, S., Kobayashi, T., 2013. Bloch simulations towards direct detection of oscillating magnetic fields using MRI with spin-lock sequence. Conf. Proc. IEEE Eng. Med. Biol. Soc. 2013, 1061–1064.
Ogawa, S., Lee, T.M., Kay, A.R., Tank, D.W., 1990. Brain magnetic resonance imaging with contrast dependent on blood oxygenation. Proc. Natl. Acad. Sci. U. S. A. 87, 9868–9872.
Park, T.S., Lee, S.Y., Park, J.H., Lee, S.Y., 2004. Effect of nerve cell currents on MRI images in snail ganglia. Neuroreport 15, 2783–2786.
Petridou, N., Plenz, D., Silva, A.C., Loew, M., Bodurka, J., Bandettini, P.A., 2006. Direct magnetic resonance detection of neuronal electrical activity. Proc. Natl. Acad. Sci. U. S. A. 103, 16015–16020.
Pfeuffer, J., Van de Moortele, P.F., Ugurbil, K., Hu, X., Glover, G.H., 2002. Correction of physiologically induced global off-resonance effects in dynamic echo-planar and spiral functional imaging. Magn. Reson. Med. 47, 344–353.
Pisauro, M.A., Dhruv, N.T., Carandini, M., Benucci, A., 2013. Fast hemodynamic responses in the visual cortex of the awake mouse. J. Neurosci. 33, 18343–18351.
Rager, G., Singer, W., 1998. The response of cat visual cortex to flicker stimuli of variable frequency. Eur. J. Neurosci. 10, 1856–1877.
Ritter, P., Villringer, A., 2006. Simultaneous EEG-fMRI. Neurosci. Biobehav. Rev. 30, 823–838.
Schulz, K., Sydekum, E., Krueppel, R., Engelbrecht, C.J., Schlegel, F., Schroter, A., Rudin, M., Helmchen, F., 2012. Simultaneous BOLD fMRI and fiber-optic calcium recording in rat neocortex. Nat. Methods 9, 597–602.
Silva, A.C., Koretsky, A.P., Duyn, J.H., 2007. Functional MRI impulse response for BOLD and CBV contrast in rat somatosensory cortex. Magn. Reson. Med. 57, 1110–1118.
Singh, M., 1994. Sensitivity of MR phase shift to detect evoked neuromagnetic fields inside the head. IEEE Trans. Nucl. Sci. 41, 349–351.
Sundaram, P., Wells, W.M., Mulkern, R.V., Bubrick, E.J., Bromfield, E.B., Munch, M., Orbach, D.B., 2010. Fast human brain magnetic resonance responses associated with epileptiform spikes. Magn. Reson. Med. 64, 1728–1738.
Wheaton, A.J., Borthakur, A., Corbo, M.T., Moonis, G., Melhem, E., Reddy, R., 2004. T2rho-weighted contrast in MR images of the human brain. Magn. Reson. Med. 52, 1223–1227.
Witschey II, W.R., Borthakur, A., Elliott, M.A., Mellon, E., Niyogi, S., Wallman, D.J., Wang, C., Reddy, R., 2007. Artifacts in T1 rho-weighted imaging: compensation for B(1) and B(0) field imperfections. J. Magn. Reson. 186, 75–85.
Witzel, T., Lin, F.H., Rosen, B.R., Wald, L.L., 2008. Stimulus-induced Rotary Saturation (SIRS): a potential method for the detection of neuronal currents with MRI. Neuroimage 42, 1357–1365.
Xiong, J., Gao, J.H., Lancaster, J.L., Fox, P.T., 1995. Clustered pixels analysis for functional MRI activation studies of the human brain. Hum. Brain Mapp. 3, 287–301.
Xiong, J., Fox, P.T., Gao, J.H., 2003. Directly mapping magnetic field effects of neuronal activity by magnetic resonance imaging. Hum. Brain Mapp. 20, 41–49.
Xue, Y., Chen, X., Grabowski, T., Xiong, J., 2009. Direct MRI mapping of neuronal activity evoked by electrical stimulation of the median nerve at the right wrist. Magn. Reson. Med. 61, 1073–1082.